Sensors and Actuators B 149 (2010) 136–142

Contents lists available at ScienceDirect

Sensors and Actuators B: Chemical

journal homepage: www.elsevier.com/locate/snb

A capacitive humidity sensor based on ordered macroporous silicon with thin film surface coating

Yun Wang[a], Seungwoo Park[a], John T.W. Yeow[a,*], Andreas Langner[b], Frank Müller[b]

[a] Systems Design Engineering, University of Waterloo, 200 University Avenue West, Waterloo, Ontario, N2L 6P6, Canada
[b] Max Planck Institute of Microstructure Physics, Weinberg 2, 06120 Halle (Saale), Germany

ARTICLE INFO

Article history:
Received 21 December 2009
Received in revised form 3 May 2010
Accepted 8 June 2010
Available online 15 June 2010

Keywords:
Humidity sensor
Ordered structure
Ordered macroporous silicon
Ta_2O_5

ABSTRACT

In this paper, we report a new approach for humidity sensing. The sensor is based on ordered macroporous silicon with a Ta_2O_5 thin film coating. The ordered macroporous silicon array has perfectly aligned pores and uniform pore size (4 μm). The 95 nm Ta_2O_5 thin film is uniformly deposited on the pore surface by atomic layer deposition (ALD), which acts as an adsorption enhancement layer. The sensor's capacitance is measured to RH changes. The sensor shows very high sensitivity and small hysteresis, especially at high RH levels. It also shows very good repeatability and long term stability.

1. Introduction

The growing awareness of global environmental and energy problems has promoted the intensive research in hydrogen fuel cells—a high efficiency and virtually pollution free energy source. However, there are technical challenges preventing the miniaturization of fuel cells and their application in vehicles and other forms of transportations [1]. Water management is one of the crucial problems of maximizing the performance of fuel cells, especially for proton-exchange membrane fuel cells (PEMFC) [2]. The PEMFC's efficiency is highly dependent on the operating conditions, including temperature, humidity and air flow rate. To obtain an optimal performance by minimizing the energy losses, the identification, monitoring, and controlling of the operating conditions play an important role in the design and operation of fuel cell systems. However, commercially available humidity sensors (mostly polymer sensors) are incapable of working in constantly high humidity environments and under high temperatures [3]. Therefore, they are not suitable for PEMFC applications. The development of micro- and nano-technology provides the opportunity to integrate micro-sensing system into the fuel cell stack for real-time monitoring and controlling of the system—thereby improving the performance of the overall system. The motivation of our work is to design and fabricate a micro humidity sensor that is capable of working in high relative humidity (RH) conditions with long term stability.

In this paper, we introduce a new approach for humidity sensing. Ordered macroporous silicon with a uniform metal oxide coating is used as the gas sensing material. Both porous silicon (PS) and metal oxides, especially nanostructured metal oxides, are commonly used gas sensing materials due to their high surface-to-volume ratio [4–8]. When compared to polymers, they have shown relatively good thermal and chemical stability. However, the difficulty of fabricating these materials reliably and consistently is one of the biggest challenges in their real life application. In the conventional application of PS in gas sensors, PS has a random aligned and interconnected structure. These features induce capillary condensation and a long recovery time. Ordered macroporous silicon, on the other hand, has uniform pore size, shape and distribution. All pores are aligned vertically and are open to the ambient environment, which significantly increases the adsorption efficiency of gas molecules onto the porous structure. In addition, the surface area and porosity of ordered macroporous silicon can be precisely controlled. Therefore, a better gas sensing property can be achieved by adjusting the etching parameters. Furthermore, uniform deposition or growth of surface coating on this pore array is easier and more controllable.

To improve the adsorption of water molecules on the sensing surface, a thin film layer of Ta_2O_5 is deposited on top of the porous structure uniformly. Ta_2O_5 is a semiconducting metal oxide with a high dielectric constant. It has been used as chemical sensing mate-

* Corresponding author.
E-mail address: jyeow@engmail.uwaterloo.ca (J.T.W. Yeow).

0925-4005/$ – see front matter © 2010 Elsevier B.V. All rights reserved.
doi:10.1016/j.snb.2010.06.010

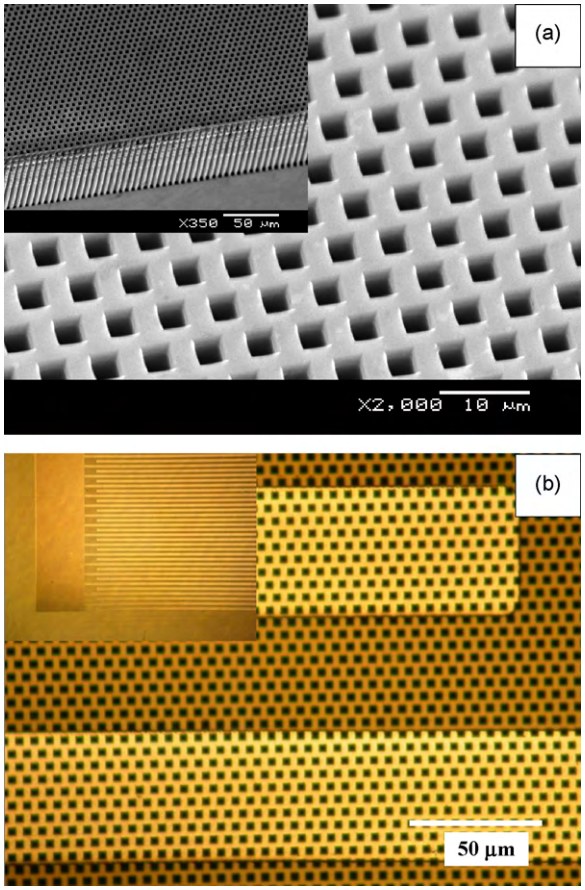

Fig. 1. (a) Profile SEM image of a 3D ordered macroporous silicon with square pores (1 μm in diameter); (b) a microscope image of the Al electrodes on top of the PS; the inset is a view of the interdigitated electrodes of the sensor.

rial or a promoter for other metal oxides in gas sensors [9–12]. In this ordered macroporous silicon humidity sensor, it acts as the water adsorption enhancing layer due to its very small water contact angle.

2. Sensor fabrication and measurement setup

The ordered macroporous silicon is prepared by electrochemical etching of (1 0 0)-oriented n-type Si in hydrofluoric acid (HF) with backside illumination. The Si wafer is initially pre-patterned by photolithography and then etched in KOH to define the nucleation spots of the pores. To fit into the etch cell, the wafer is then cleaved into 23 mm × 23 mm pieces. The detailed etching parameters were reported previously [13]. The porous area is 20 mm in diameter. The ordered structure can have a pore diameter of 1–4 μm, and pore-to-pore distance of to 6 μm. The length of the pores can be controlled by the etch time and reach 200 μm without any degradation of the order and sidewall uniformity. Fig. 1 shows a 3D view of the ordered porous structure with perfectly aligned pores and high aspect ratio.

The porous structured used in this sensor has a pore size of 4 μm and pore depth of 97 μm. The 23 mm × 23 mm sample is cleaved into half. The Ta_2O_5 thin film is then deposited uniformly on the macroporous silicon surface by atomic layer deposition (ALD) and has a thickness of 95 nm. The interdigitated electrodes are fabricated on top of the sensor by lift-off process. Due to the macroporous structure, the commonly used thin photoresist (PR) is not sufficient to cover the pores. Therefore, AZP4330 is used for the lithography. The PR is spun onto the sample with a rotational rate

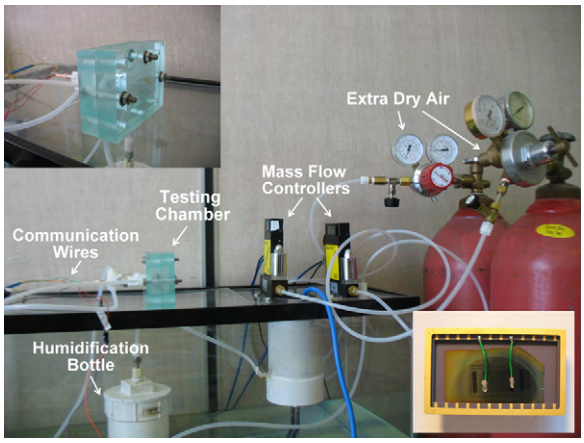

Fig. 2. Experiment setup; inset (up-left) the testing chamber and (lower right) a picture of the as fabricated humidity sensor.

of 1000 rpm for 60 s. The thickness of the PR on top of the porous area is 1–2 μm while it is 7–10 μm on the smooth edge area. MF322 is used as the developer. After photolithography, 250 nm Al is evaporated onto the sample. The sensor is then assembled into a chip carrier and wirebonded by soldering.

The sensor is placed in a sealed chamber with controllable RH and temperature. The chamber has two gas inlets and one outlet. One inlet connects to extra dry air. The other inlet is connected to a humidification chamber where the extra dry air becomes saturated with water vapor. Two mass flow controllers are implemented to control the flow rate of the dry and saturated air respectively. As a result, the RH in the chamber can change continuously from 0% to 100% (with 2–3% error). A commercial humidity sensor is placed in the chamber as a reference indictor of the RH level. Real-time measurement is performed with a LRC/ESR meter (PK PRECISION 889A). A LabVIEW program is used for device controlling and data acquisition. Fig. 2 shows the measurement setup. The inset is an image of the as fabricated humidity sensor. The sensor is 23 mm × 11 mm and the chip carrier is 33 mm × 20 mm. All the measurements in this paper are performed under room temperature.

3. Results

3.1. Sensitivity

Capacitance measurement is performed to evaluate the sensor's behavior to humidity changes. The measurement voltage is 1 V. The measurement frequency ranges from 100 Hz to 200 kHz. In this report, we define the percentage capacitance variation (PCV) at a certain RH level as,

$$\mathrm{PCV}_{@\mathrm{RH\%}} = \frac{(Cp_{@\mathrm{RH\%}} - Cp_0) \times 100\%}{Cp_0} \quad (1)$$

We define the sensor's sensitivity (S) as,

$$S = \frac{\Delta Cp}{\Delta \mathrm{RH}} \quad (2)$$

Where $Cp_{@\mathrm{RH\%}}$ is the capacitance of the sensor at a certain RH level and Cp_0 is the original capacitance reading of the sensor at 0% RH.

The sensor's capacitance is measured by changing RH from 0% to 100% in incremental steps. Each step is maintained at a constant value till the capacitance reading reaches a steady value. Fig. 3 shows the sensor's capacitance response to RH. Fig. 3(a) shows the PCV response to RH changes, while Fig. 3(b) shows the actual capacitance variations to RH changes. As observed in Fig. 3, the sensor's capacitance increases significantly with increasing RH at all measuring frequencies, especially at high RH. When RH increases from

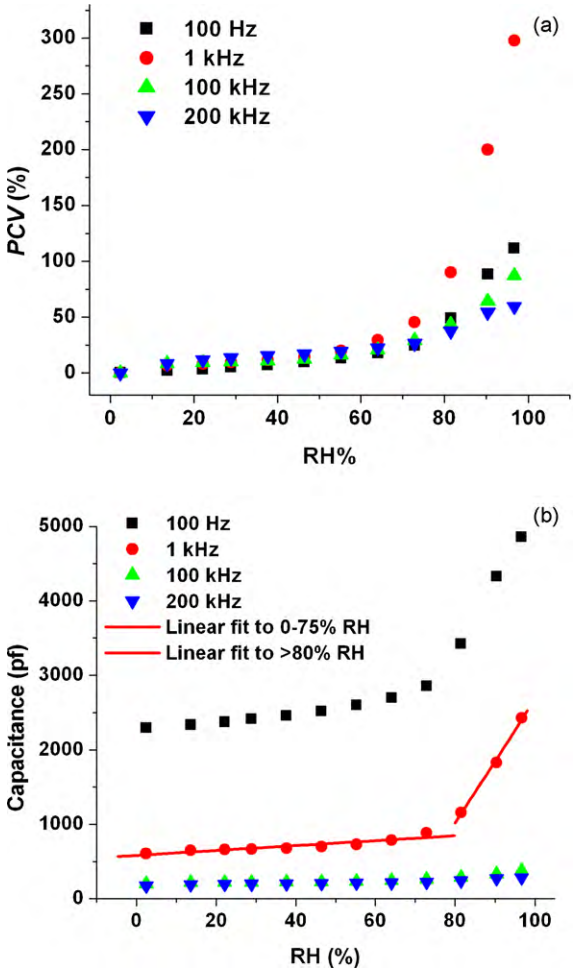

Fig. 3. (a) PCV–RH curve and (b) *Cp*–RH curve at different measurement frequencies.

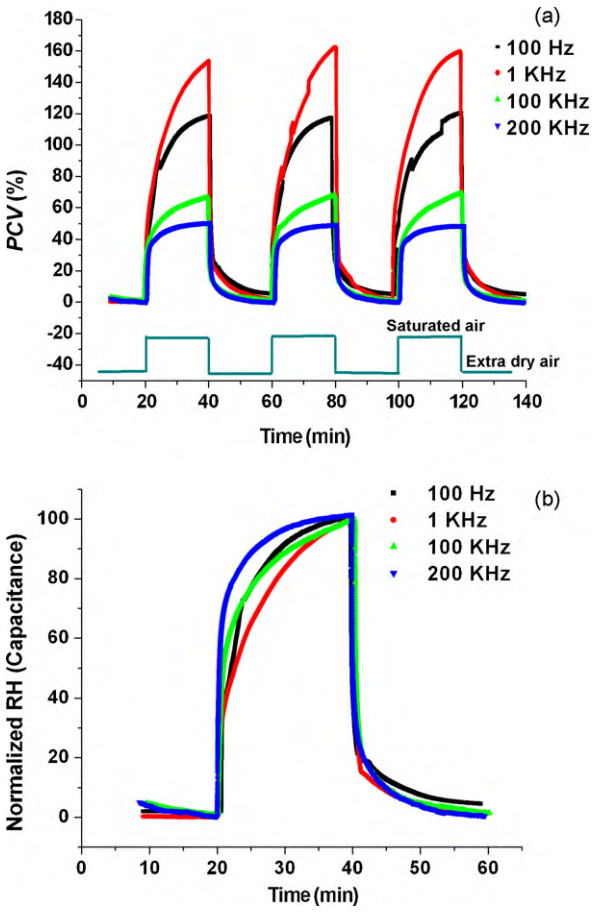

Fig. 4. (a) Dynamic capacitance response between extra dry and saturated air at different test frequencies; (b) normalized dynamic capacitance response between extra dry and saturated air at different test frequencies.

0% to 64%, the PCV is within the same range (17–23%) for all frequencies. As the RH continues to increase, the sensor shows larger PCV under lower operation frequency. The sensor shows the highest overall PCV at 1 kHz, which is 297.5% from 0% to 100% RH. The lowest overall PCV is 59.6% at 200 kHz. The reason for the PCV differences at different operation frequencies will be discussed in the next section.

Although the *Cp*–RH curves are not linear in the full RH range from 0% to 100%, the curves can be divided into two regions: 0–75% RH and 80–100% RH. In both regions, the sensor exhibits very good linearity. In Fig. 3(b), it shows the linear fit curves of the experiment data measured at 1 kHz in these two regions. To perform the linear fit, we set the confidence interval to be 95%. The results show that the correlation coefficient (R) is 0.921 and 0.998 for region 0–75% and region 80–100% respectively. The p-value (probability that R is zero) is 4.2E−4 and 0.04 respectively, indicating very good linearity of the data. The sensor's sensitivity at 1 kHz is 3.3 pf/RH in the 0–75% region and 83.2 pf/RH in the 80–100% region.

3.2. Response time

One important parameter to assess humidity sensors or any other chemical sensors is the response time. Fig. 4(a) demonstrates the sensor's dynamic responses to cycle changes of RH between extra dry air and saturated air at different measuring frequencies. To compare the performance of the sensor at different frequencies, each step is kept for a 20 min duration. The sensor shows very good repeatability from cycle to cycle at all frequencies. An immediate change of the capacitance is observed on both increasing and decreasing RH cycles. We observe that the sensor shows different response time under different frequencies. Compare Figs. 4(a) and 3(a), at measuring frequency of 100 Hz, 100 kHz and 200 kHz, the sensor reaches its maximum PCV within the 20 min after the RH level increases from 0% to 100%. However, when operating at 1 kHz, the sensor's PCV reaches 153.5% in 20 min while its maximum PCV at 100% RH is 297.5%. This means the sensor has much longer response time when operating at 1 kHz.

It has been demonstrated that, capacitance/impedance measurement can truly reflect and monitor the actual state of ad- or desorption process in a porous sorbent [14]. To compare the ad-/desorption process at different measuring frequency more clearly, Fig. 4(b) shows the normalized dynamic response of one of the cycles in Fig. 4(a). It can be seen that, while the desorption processes follow very similar path at different frequencies, the adsorption processes vary significantly. The adsorption slows down much earlier at 1 kHz. This observation has been confirmed by repeatable results. To better understand this phenomenon, the dynamic impedance response of the sensor is also measured with the same LRC meter at different frequencies. Fig. 5 shows the normalized dynamic impedance response at different frequencies when RH increases from 0% to 100%. While the capacitance of the sensor increases with increasing RH level, its impedance decreases [15]. However, the sensor shows very similar adsorption path with the capacitance response at each frequency. The sensor always shows the fastest response time (the time that the sensor takes to achieve 90% of the total change) at 200 kHz.

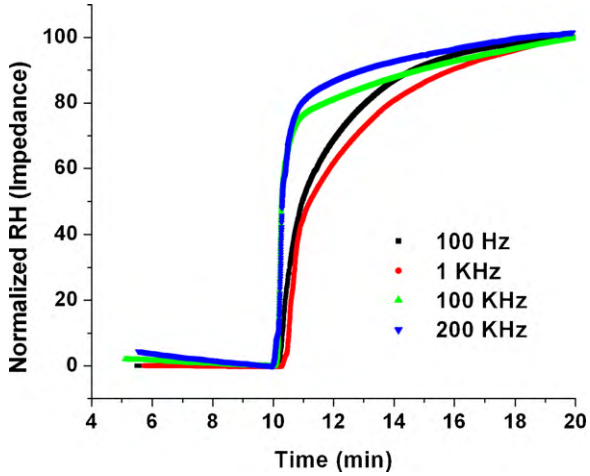

Fig. 5. Normalized dynamic impedance response between extra dry and saturated air at different measuring frequencies.

At this moment, the mechanism behind this response time-frequency dependence observation is not clear yet. It has been proven that external electric field can affect the molecule's (both polar and non-polar) adsorption on the sorbent surface [16,17]. Kunishima et al. [18] found that Cl_2 adsorption on SnO_2 film is much faster under negative bias voltage than that under positive bias or no bias voltage. We believe that the alternating electric field has effect on both the interactions between the water molecules and sorbent surface and the interactions between the adsorbed molecules themselves. As a result, the sensor shows different adsorption paths at different frequencies. Fig. 6(a) and (b) shows the sensor's normalized capacitance response to RH changes between 0% and 38%, and between 0% and 73% at three different frequencies. It can be seen that the differences in the adsorption paths are much smaller at low RH level. Since the differences in adsorption path are more pronounced at high RH level, where multilayer of water molecules is formed, the effect on the interactions between adsorbed water molecules seems to be more dominating. More investigation is undergoing to fully understand this phenomenon. It is noticeable that the dynamic curves to the changes between 0% RH and 73% RH in Fig. 6(b) is slightly different from the other dynamic curves. The change of the capacitance slows down in the middle and then accelerates again. We believe that this is where the surface is fully covered with water molecules and multilayer of molecules starts to form. This also results in the increase of the sensor's sensitivity at high RH level.

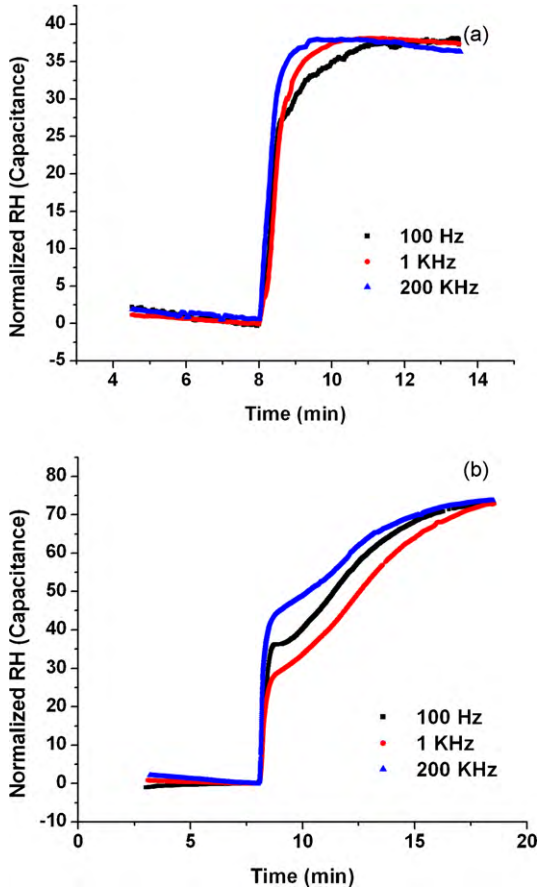

Fig. 6. (a) Dynamic capacitive response to RH changes between 0% and 38%; (b) dynamic capacitive response to RH changes between 0% and 73%.

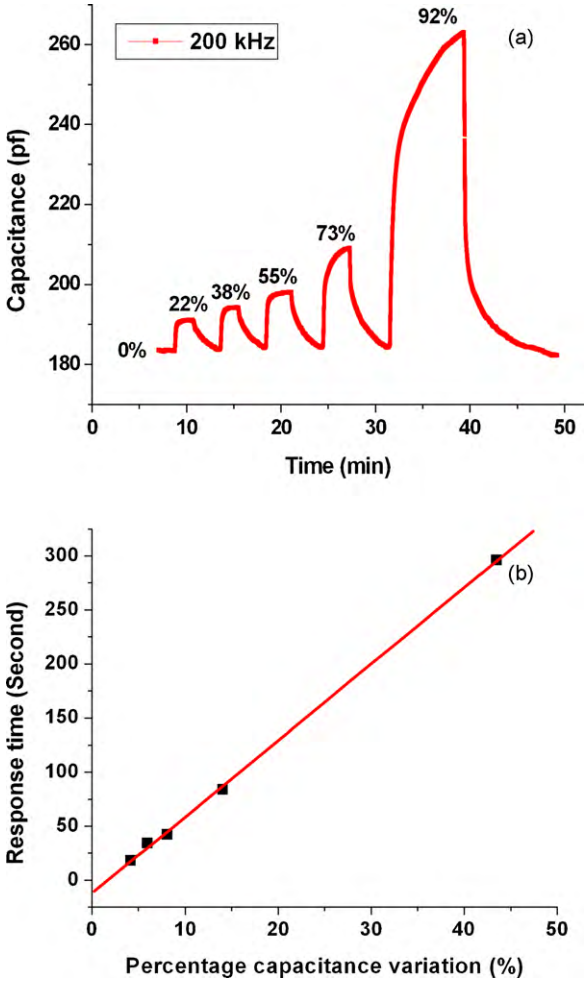

Fig. 7. (a) Dynamic response of the sensor to different RH% levels under 200 kHz; (b) the relationship of the response time from 0% to certain RH level to PCV under 200 kHz.

The sensor's response time also depends on the change of RH level Fig. 7(a) shows the dynamic capacitance response of the sensor between 0% RH and different RH levels at 200 KHz. When the RH increases from 0% to 22%, the sensor reaches 90% of the total change in 18 s. When RH increases from 0% to a higher RH, the response time slightly increases accordingly. This can be explained by the nature of the diffusion and adsorption process. When the RH changes to a higher level, there are more water molecules to diffuse into the structure and adsorb onto the sensing surface. This results

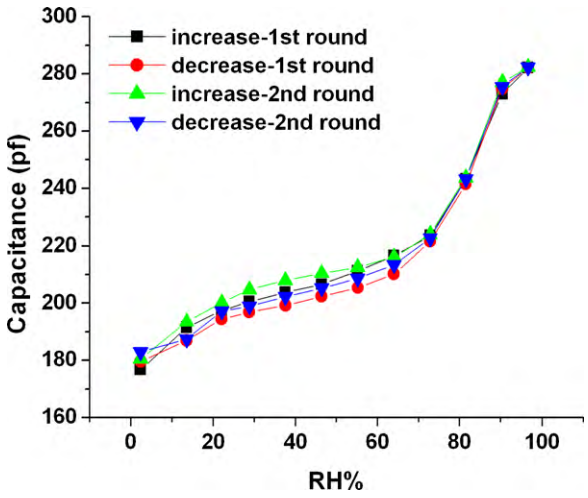

Fig. 8. The capacitance–RH curve with step up and step down RH changes at 200 kHz.

in longer response time and higher capacitance change. Fig. 7(b) proves this interpretation by showing the linear relationship of the sensor's response time to the PCV corresponding to the RH level in Fig. 7(a). Since the RH in the environmental chamber is changed by flowing dry or wet air, the RH does not reach the desired level immediately. This can contribute to part of the response time as well.

3.3. Stability and hysteresis

The sensor was stored in air at room temperature for several months before the electrode fabrication and soldering. The sensor is tested repeatedly under different RH levels for more than three months. The sensor is predominately tested at high RH levels. During the test, the sensor shows very good stability and repeatability. Fig. 8 shows the *Cp*–RH curves at 200 kHz for two round tests which are performed on two different days. The data show very good consistency. This is also observed for the other frequencies.

Hysteresis is another common issue with gas sensors. The sensor is tested with increasing and decreasing RH steps and shows very small hysteresis, especially at high RH. The hysteresis is 0.3–3.3% over the whole RH range. Since the target application of this sensor is for high humidity environment, the sensor's behavior is tested

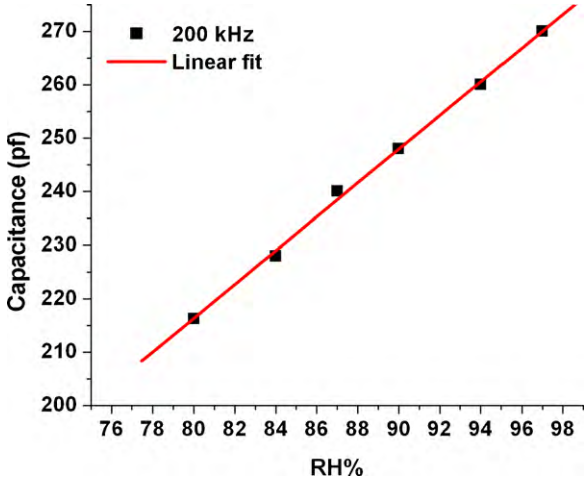

Fig. 9. The *Cp*–RH curve between 80% and 100% RH at 200 kHz.

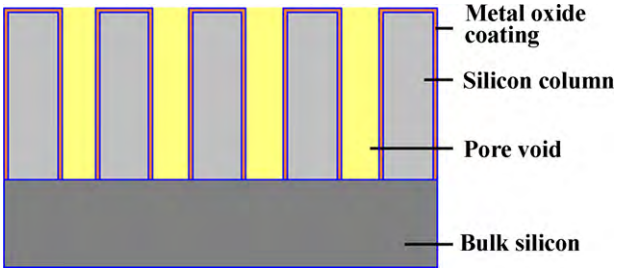

Fig. 10. the structure of ordered PS with metal oxides thin film coating on the surface.

with finer RH steps. Fig. 9 shows the *Cp*–RH curve between 80% and 100% RH with 6 steps at 200 kHz. The sensor shows perfect linearity over this range. The sensitivity is in this range is 3.2 pf/RH.

4. Discussions

The capacitance response of porous structures is often attributed to the replacement of air with adsorbed water molecules in the pores [19]. For conventional random aligned PS, it is hard to build an exact model to represent the structure. Rittersma and Benecke [20] used a simple model that considers random PS layers as a uniform network of partly oxidized Si nanowires and voids, as shown in Fig. 10. This is very similar with the order macroporous structure that is used in this experiment, except for that the pores are not connected with each other.

When the PS is exposed to water vapor, water molecules will be adsorbed on the metal oxide surface. For most metal oxides, both chemisorption and physical adsorption occur upon exposure to moisture [21]. At low RH, a monolayer of water molecules is initially chemisorbed due to the electron vacancies on the surface. As the RH increases, layers of physical adsorbed water molecule continue to build up on the chemisorbed layer. Since the pore size of the PS in this experiment is much larger than the Kelvin radius [13], no capillary condensation will occur at high RH levels. Therefore, when RH decreases, desorption of water molecules does not require much extra energy. This explains the sensor's very small hysteresis and fast recovery time.

Applying generalized effective medium approximation (GEMA) to the order macroporous silicon dielectric layer as shown in Fig. 10, its effective dielectric constant (ε_{PS}) with adsorbed water layers can be expressed as [18,22]

$$\frac{1-p}{1-r}\frac{\varepsilon_{Si}^{1/t}-\varepsilon_{PS}^{1/t}}{\varepsilon_{Si}^{1/t}+(\varphi_P/(1-\varphi_P))\varepsilon_{PS}^{1/t}}+\frac{r(1-P)}{1+r}\frac{\varepsilon_{MOw}^{1/t}-\varepsilon_{PS}^{1/t}}{\varepsilon_{MOw}^{1/t}+(\varphi_P/(1-\varphi_P))\varepsilon_{PS}^{1/t}}+\varphi_w P\frac{\varepsilon_w^{1/t}-\varepsilon_{PS}^{1/t}}{\varepsilon_w^{1/t}+(\varphi_P/(1-\varphi_P))\varepsilon_{PS}^{1/t}}+(1-\varphi_w)P\frac{\varepsilon_A^{1/t}-\varepsilon_{PSw}^{1/t}}{\varepsilon_A^{1/t}+(\varphi_P/(1-\varphi_P))\varepsilon_{PS}^{1/t}}=0 \quad (3)$$

where ε_{Si}, ε_{MOw}, ε_A, and ε_w are the dielectric constants of the silicon, metal oxide in moisture environment, air, and water respectively; P is the porosity of the structure, r is the volume ratio of the metal oxide and Si, φ_w is the fractional volume of the adsorbed water vapor layers on the surface in the pore space, φ_P is the percolation volume fraction and t is the non-linearity correction factor.

When there are layers of adsorbed water vapor in the pore space, φ_w will increase from 0 to 1. Since water has very high dielectric constant at room temperature (80) compare to air (1), the effective dielectric constant of the PS will increase accordingly. It is also shown in Eq. (3) that the dependence of capacitance on RH level

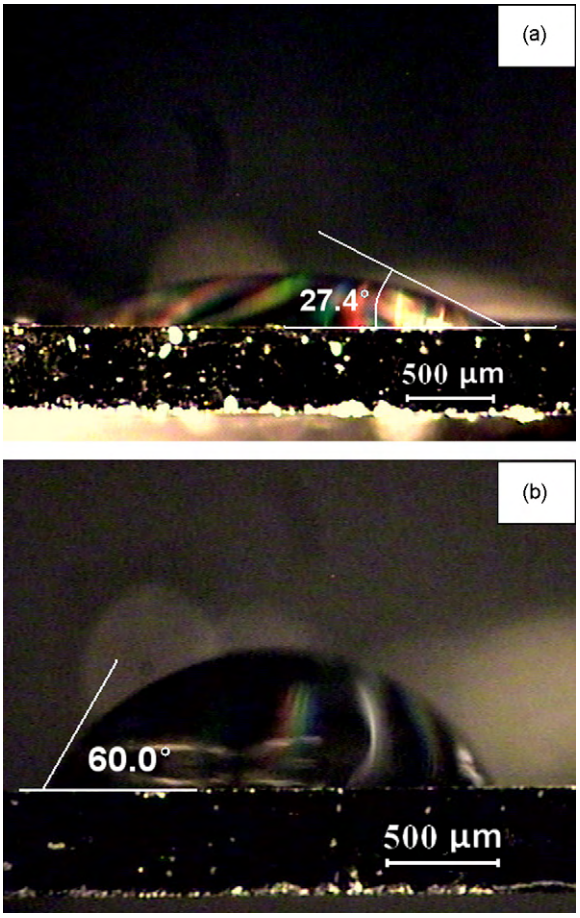

Fig. 11. Measurement of water contact angle of (a) Ta_2O_5 thin film coated silicon surface; (b) bare silicon surface. The measurement is taken at non-porous area of the sensors in a 3D micro-stage system with horizontally aligned microscope.

can be controlled by adjusting the porosity and the thickness of the metal oxide layer.

The dependence of the capacitance variation on the measurement frequency can be explained by the existence of parasitic capacitance. The parasitic capacitance is generally from the bulk silicon and the interfaces between different layers. It is not affected by the RH change. Through modeling, Das et al. [19] demonstrated that at very high frequencies, the measured capacitance is mainly determined by the parasitic capacitance. On the other hand, at low frequencies, the measured capacitance truly represents the active capacitance for humidity sensing. Therefore, the measured capacitance variation is higher at lower operation frequency. This is consistent with our experiment results. The sensor showed the highest *Cp* variation at 100 Hz. It is 2563 pf at 100 Hz, while the *Cp* variation is 1815 pf, 176 pf, and 105 pf at 1 kHz, 100 kHz and 200 kHz respectively.

The enhancement effect of the Ta_2O_5 thin film coating on the sensor's performance is mainly due to its ultra-hydrophilic property. Fig. 11(a) and (b) shows the water contact angle of Ta_2O_5 thin film coated silicon surface compare to bare silicon surface (with 3 nm native SiO_2). The Ta_2O_5 thin film coated surface shows a very small contact angle. Previously, we reported the sensing properties of ordered macroporous silicon with different surface coatings, including bare Si, thermally grown SiO_2 (100 nm), ALD deposited ZnO (100 nm) and HfO_2 (100 nm) [13]. Table 1 gives the comparison of their water contact angle and maximum PCV (obtained under different measuring frequency since the difference in their parasitic capacitance). It shows that the sensor with coatings that

Table 1
Comparison of the water contact angle and PCV (%) of ordered macroporous silicon humidity sensor with different surface coatings.

Surface coating	Contact angle (°)	PCV (%)
Ta_2O_5	27.4	300
Si	60.0	13.9
HfO_2	66.5	55
ZnO	80.1	1.8
SiO_2	88.6	0.36

are more hydrophilic have better sensitivities. We believe that the interactions between the adsorbed water molecules and the Ta_2O_5 or HfO_2 coatings also partially contribute to the higher sensitivity. This explains the higher PCV of HfO_2 coated sensor than the PCV of bare Si sensor, although it has slightly larger contact angle.

5. Conclusions

In this paper, we demonstrated the humidity sensing characteristic of a Ta_2O_5 thin film enhanced ordered macroporous silicon humidity sensor. The sensor's capacitance response to RH changes is measured at different frequencies. When the RH increases, the sensor's capacitance increases with a fast response time. The sensor's *Cp*–RH relationship shows perfect linearity in two regions respectively over the whole RH range. The capacitance change upon exposure to moisture is mainly caused by the replacement of air with adsorbed water molecules in the pore space. Due to the existence of parasitic capacitance, the sensor exhibits a higher capacitance variation values at low frequencies. The sensor shows the fastest response time at 200 kHz. More investigation is needed to explain this dependency of response time on measuring frequency. To achieve a fast response and relatively high sensitivity, a frequency of 200 kHz is chosen as the operation frequency of the sensor. At 200 kHz, the response time is 18–40 s to small RH changes, while it is 300 s to 100% RH changes. The sensor shows very good linearity, repeatability and long term stability. The hysteresis at 200 kHz is 0.3–3.3%. Overall, the sensor shows great potential for the application in PEMFC.

Acknowledgment

The author would like to thank NSERC for the financial support.

References

[1] A. Boudghene Stambouli, E. Traversa, Fuel cells, an alternative sources of energy, Renew. Sust. Energy Rev. 6 (2002) 295–304.
[2] S. Vengatesan, H.-J. Kima, E.A. Cho, et al., Operation of a proton-exchange membrane fuel cell under non-humidified conditions using thin cast Nafion membranes with different gas-diffusion media, J. Power Sources 156 (2006) 294–299.
[3] J.H.-S. Michael, J. Ervin, M. Andersen, Anodic nano-porous humidity sensing thin films for the commercial and industrial applications, IEEE IAS (2004) 1207–1210.
[4] B. Coasne, A. Grosman, N. Dupont-Pavlovsky, C. Ortegaa, M. Simon, Adsorption in an ordered and non-interconnected mesoporous material: single crystal porous silicon, Phys. Chem. Chem. Phys. vol. 3 (2001) 1196–1200.
[5] G. Barillaro, P. Bruschi, F. Pieri, L.M. Strambini, CMOS-compatible fabrication of porous silicon gas sensors and their readout electronics on the same chip, Phys. Status Solidi A 204 (2007) 1423–1428.
[6] E. Galeazzo, H.E.M. Peres, G. Santos, N. Peixoto, F.J. Ramirez- Fernandez, Gas sensitive porous silicon devices: responses to organic vapors, Sens. Actuators B 93 (2003) 384–390.
[7] A. Foucaranm, B. Sorli, M. Garcia, et al., Porous silicon layer coupled with thermoelectric cooler: a humidity sensor, Sens. Actuators A 79 (2000) 189–193.
[8] G. Korotcenkov, Metal Oxides for solid-state gas sensors: what determines our choice, Mater. Sci. Eng. B 139 (2007) 1–23.
[9] Y. Ito, Long-term drift mechanism of Ta_2O_5 gate pH-ISFETs, Sens. Actuators B 64 (2000) 152–155.
[10] D.H. Kwon, B.W. Cho, C.S. Kim, et al., Effects of heat treatment on Ta_2O_5 sensing membrane for low drift and high sensitivity pH-ISFET, Sens. Actuators B 34 (1996) 441–445.

[11] H. Steffes, E. Obermeier, $In_xO_yN_z$ films with a Ta_2O_5 promoter for the detection of CO, H_2 and CH_4, Sens. Actuators B 95 (2003) 252–257.
[12] M. Kudo, T. Kosaka, Y. Takahashi, et al., Sensing functions to NO and O_2 of Nb_2O_5- or Ta_2O_5-loaded TiO and ZnO, Sens. Actuators B 69 (2000) 10–15.
[13] Y. Wang, J.T.W. Yeow, Humidity sensing of ordered macroporous silicon with HfO_2 thin film surface coating, IEEE Sens. J. 9 (2009) 541–547.
[14] J. Keller, R. Staudt, Gas Adsorption Equilibria: Experimental methods and Adsorption Isotherms, Springer, New York, 2005, pp. 344–348.
[15] M. Björkqvist, J. Paski, J. Salonen, et al., Temperature dependence of thermally-carbonized porous silicon humidity sensor, Phys. Stat. Sol. (a) 202 (8) (2005) 1653–1657.
[16] J. Keller, R. Staudt, Gas Adsorption Equilibria: Experimental methods and Adsorption Isotherms, Springer, New York, 2005, p. 299.
[17] A.B. Golovanchikov, M.Yu. Efremov, E.V. Safonov, Gas adsorption in electric field, Theoretical Foundations of Chemical Engineering 37 (5) (2003) 514–516.
[18] Y.N. Kunishima, M. Miyayama, H. Yanagida, Effects of the external electric field from a substrate on Cl_2 gas adsorption on SnO_2 thin films, Appl. Phys. Lett. 69 (1996) 632–634.
[19] J. Das, S.M. Hossain, S. Chahraborty, Role of parasitic in humidity sensing by porous silicon, Sens. Actuators A 94 (2001) 44–52.
[20] Z.M. Rittersma, W. Benecke, A humidity sensor featuring a porous silicon capacitor with an integrated refresh resistor, Sens. Mater. 12 (2000) 35–55.
[21] B.C. Yadav*, R. Srivastava, C.D. Dwivedi, Synthesis and characterization of ZnO–TiO_2 nanocomposite and its application as a humidity sensor, Philos. Mag. 88 (2008) 1113–1124.
[22] D.S. Mclachlan, The complex permittivity of emulsions: an effective media-percolation equation, Solid State Commun. 72 (1989) 831–834.

Biographies

Yun Wang (S'08) received the BSc degree in material science and engineering and the MSc degree in microelectronics and solid-state electronics from Shanghai Jiao Tong University, Shanghai, China, in 2003 and 2006, respectively. She is currently working towards the PhD degree at the Department of Systems Design Engineering, University of Waterloo, Waterloo, ON, Canada. Her current research interests are developing novel humidity sensing systems for the application on water management in fuel cell stacks.

Seungwoo Park received the BSc and MSc degrees in mechanical engineering from Sogang University, Korea, in 2007 and 2009, respectively. He is currently pursuing the PhD degree in systems design engineering at the University of Waterloo, Canada. His research interests include humidity sensors based on micro-/nano-technology.

John Yeow (S'99–M'04–SM'08) received the BSc degree in electrical and computer engineering, and MSc and PhD degrees in mechanical and industrial engineering from the University of Toronto, Toronto, ON, Canada, in 1997, 1999, and 2003, respectively. He is currently an associate professor and Canada Research Chair in Micro/Nanodevices in the Department of Systems Design Engineering at University of Waterloo, Waterloo, ON, Canada. His current research interests are in the field of developing miniaturized biomedical instruments and a wide range of sensing devices. He is a recipient of the Professional Engineering Ontario Engineering Medal, Natural Science & Engineering Research Canada Innovation Challenge Award, Douglas R. Colton's Medal of Research Excellence, Micralyne Microsystems Design Award, Ontario Ministry of Research and Innovation's Early Researcher Award, and University of Toronto Alumni Association 7T6 Early Career Award. He is the Editor-in-Chief of the IEEE Nanotechnology Council Newsletter. He is also an Associate Editor of the IEEE Nanotechnology Magazine.

Andreas Langner received his diploma degree in physics from the Humboldt-University in Berlin (2004) and his PhD degree from the Martin Luther University in Halle-Wittenberg (2008). In his PhD work at the Max Planck Institute of Microstructure Physics he focused on the fabrication and application of macroporous silicon. Presently he is working on the fabrication of nanostructures using the EUV interference lithography beamline at the Paul Scherrer Institute, Switzerland.

Frank Müller obtained his PhD. from the Technical University of Munich in 1993. The topic of his dissertation was infrared spectroscopy on 2D electron gas systems and on microporous silicon. He then joint the group of Prof. Ulrich Gösele at the newly founded Max-Planck-Institute of Microstructure Physics in Halle, where he is dealing with the preparation of ordered porous materials (mainly silicon and alumina) and their applications.